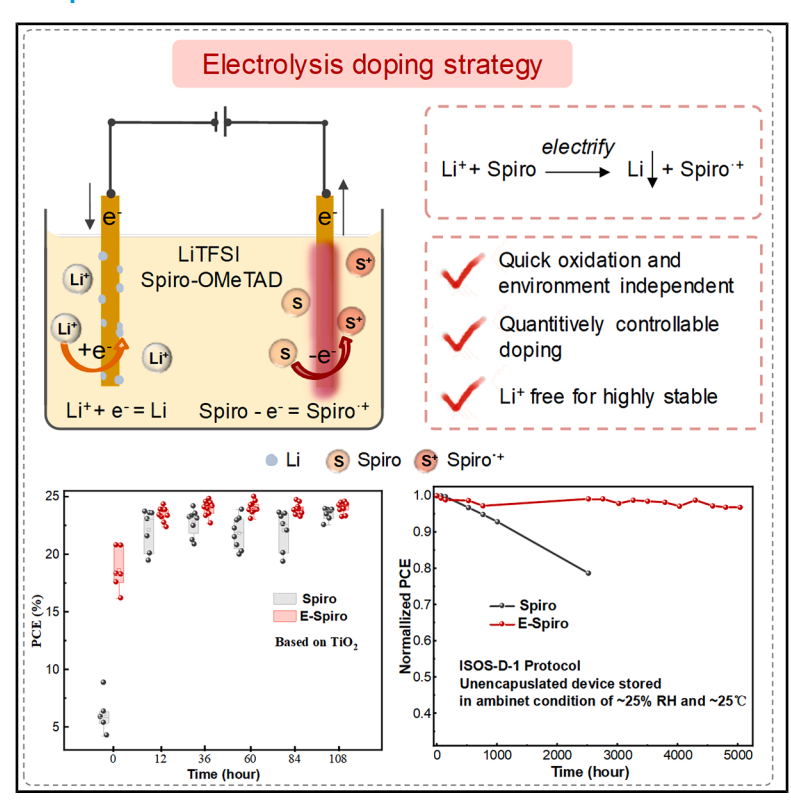


# Controllable electrolysis doping of organic semiconductors for stable perovskite solar cells

# **Graphical abstract**



# **Highlights**

- A novel electrolysis doping strategy to modulate organic semiconductors
- Achieving controllable doping with negligible residual Li<sup>+</sup>
- PCEs of 26.12% and 25.57% are achieved for regular and inverted PSCs, respectively
- Device maintains >90% of initial PCE after 1,000 hours of operation

## **Authors**

Hao Huang, Zhineng Lan, Yingying Yang, ..., Benyu Liu, Peng Cui, Meicheng Li

# Correspondence

mcli@ncepu.edu.cn

# In brief

The organic hole transport layers (normally including LiTFSI) in perovskite solar cells suffer a complex, timeconsuming oxidation process accompanied by massive residual Li<sup>+</sup> to obtain optimal electrical properties. In this work, we proposed a novel electrolysis doping strategy to modulate organic semiconductors, enabling controllable doping and effective Li\* removal. As a result, the regular perovskite solar cells using electrolyzed Spiro achieved a PCE of 26.16%, and the inverted-structured perovskite solar cells using electrolyzed PTAA achieved a PCE of 25.57%.



Please cite this article in press as: Huang et al., Controllable electrolysis doping of organic semiconductors for stable perovskite solar cells, Joule (2025), https://doi.org/10.1016/j.joule.2025.102106

**Joule** 



# **Article**

# Controllable electrolysis doping of organic semiconductors for stable perovskite solar cells

Hao Huang,<sup>1,3</sup> Zhineng Lan,<sup>1,3</sup> Yingying Yang,<sup>1</sup> Huilin Yan,<sup>1</sup> Meng Wan,<sup>1</sup> Yi Lu,<sup>1</sup> Shujie Qu,<sup>1</sup> Tongtong Jiang,<sup>1</sup> Changxu Sun,<sup>1</sup> Benyu Liu,<sup>2</sup> Peng Cui,<sup>1</sup> and Meicheng Li<sup>1,4,\*</sup>

<sup>1</sup>State Key Laboratory of Alternate Electrical Power System with Renewable Energy Sources, School of New Energy, North China Electric Power University, Beijing 102206, China

CONTEXT & SCALE Perovskite solar cells (PSCs) hold great promise for the capture and utilization of solar energy. Currently, PSCs are at a critical juncture in the transition from laboratory research to practical applications. In this context, organic semiconductors, which are commonly employed as hole transport materials, play a pivotal role. However, the conventional doping method with the involvement of lithium bis(trifluoromethane)sulfonimide (LiTFSI) suffers a complex and time-consuming oxidation process accompanied by massive residual Li+, detrimentally impacting device stability. In this work, we first proposed a novel electrolysis doping strategy to modulate organic semiconductors, achieving quantitively controllable doping with negligible residual Li<sup>+</sup>. The electrolysis doping strategy subtly leverages the redox agents of hole and electron to selectively oxidize the organic semiconductor to be radical and reduce Li<sup>+</sup> to Li atom respectively, which shows a mechanism distinct from the traditional doping method using a chemical additive. This electrolysis doping exhibits a universal application in various semiconductors, such as 2,2',7,7'-Tetrakis [N,N-di(4-methoxyphenyl)amino]-9,9'-spirobifluorene (Spiro), poly[bis(4-phenyl) (2,4,6-trimethylphenyl)amine (PTAA), poly(3-hexylthiophene-2,5-diyl) (P3HT), and others. The resulting regular PSCs with electrolyzed Spiro achieve an efficiency of 26.12% with an improved storage stability by maintaining >95% of initial efficiency after aging in ambient air for 5,000 h. Furthermore, the inverted PSCs with electrolyzed PTAA achieve an efficiency of 25.57% with excellent stability by maintaining >90% of initial efficiency after operating for 1,400 h under continuous illumination in a N<sub>2</sub> atmosphere. Our work provides new technology with a distinct mechanism to modulate semiconductors, providing more opportunities for promoting PSCs' commercializa-

### **SUMMARY**

The conventional doping method of organic semiconductors (commonly including lithium bis(trifluoromethane)sulfonimide [LiTFSI]) served as hole transport layers in perovskite solar cells (PSCs) suffers from a complex, time-consuming oxidation process, detrimentally impacting device stability. Herein, we propose a novel electrolysis doping strategy to modulate organic semiconductors, enabling controllable doping and effective Li<sup>+</sup> removal. This electrolysis doping exploits holes with tunable oxidizing capabilities to oxidize organic semiconductors into ion radicals at the surface of the anode electrode, which exhibits a high reproducibility and a universal application on different organic semiconductors. Simultaneously, Li<sup>+</sup> ions can be reduced to Li atoms at the surface of the cathode electrode, thus removing stability-damaging residual Li<sup>+</sup>. Accordingly, the regular PSCs using electrolyzed 2,2',7,7'-Tetrakis[N,N-di(4-methoxyphenyl)amino]-9,9'-spirobifluorene (Spiro) achieve a power conversion efficiency (PCE) of 26.16%, and the inverted-structured PSCs using electrolyzed poly[bis(4-phenyl) (2,4,6-trimethylphenyl)amine (PTAA) achieve a PCE of 25.57% with satisfying stability by maintaining 91% of initial efficiency after operating for 1,400 h under continuous one-sun illumination.

<sup>&</sup>lt;sup>2</sup>Beijing Huairou Laboratory, Beijing 101400, China

<sup>&</sup>lt;sup>3</sup>These authors contributed equally

<sup>&</sup>lt;sup>4</sup>Lead contact

<sup>\*</sup>Correspondence: mcli@ncepu.edu.cn https://doi.org/10.1016/j.joule.2025.102106





#### **INTRODUCTION**

Metal halide perovskite solar cells (PSCs) are leading the transformation in photovoltaic technology due to their excellent semiconductor properties, such as high light absorption, long carrier diffusion length, and so on. 1-3 Along with the process updating of PSCs, the organic semiconductors, which mainly serve as the hole transport layer (HTL), have witnessed an impressive advancement of PSCs' efficiency in both regular n-i-p devices and inverted p-i-n devices. 4-6 At present, PSCs are rapidly moving forward in their cost-efficient application, in which balancing efficiency and stability is vital and necessary, determined not only by the perovskite materials but also the HTL.7-9 However, as a benchmark hole transport material on high-efficiency PSCs, 2,2',7,7'-Tetrakis[N,N-di(4-methoxyphenyl)amino]-9,9'spirobifluorene (Spiro) badly relies on the dopant of lithium bis (trifluoromethane)sulfonimide (LiTFSI) and needs a timeconsuming oxidation process to realize high conductively and suitable energy level structure. 9-12 This oxidation process, which is sensitive to ambient environment, brings a hindrance to device performance improvement and further applications.

In the conventional doping process of Spiro, the LiTFSI is utilized to facilitate the generation of Spiro radicals in ambient air with oxygen as the oxidant, thus improving the conductivity of the Spiro film. 13,14 This doping process, which is sensitive to its environment, usually requires a long period of more than 24 h to realize an optimal conductivity and Fermi level. 15,16 Besides, due to the low doping efficiency of this process, normally a large amount of LiTFSI is required to ensure the generation of enough radicals. According to the previous reports, to generate 10% radicals, ~56 mol % LiTFSI was needed to be incorporated into Spiro, with the highest proportion as residuals in the final film.<sup>17</sup> These residual lithium salts, after sufficient oxidation, show a negligible impact on film conductivity. However, they are sensitive to humidity and prone to migrate into and across the perovskite film, negatively affecting device stability. 18 Although other dopants were reported to replace LiTFSI to dope Spiro, such as the synthesized Spiro radical, 19 organic radical and ionic salts (4-tert-butyl-1-methylpyridinium bis(trifluoromethylsulfonyl)imide [TBMP+TFSI-]),9 Zn(TFSI)220 and so on,21,22 LiTFSI is still the most widely used dopant to fabricate high-efficiency PSCs. This optimal feasibility and widespread utilization of conventional doping recipe of Spiro means it is necessary and significant to address the issue of residual Li<sup>+</sup> in high-efficiency PSCs.

In addition, the conventional complex oxidation process, which is sensitive to ambient conditions, not only makes it a challenge to reveal the doping mechanism, but also makes it unable to precisely determine the practical doping amount due to the uncontrollable oxide reaction, restricting HTL optimization and design for fabricating efficient and stable PSCs. It is reported that the oxidized Spiro radical in the solid-state film can be quantified through a spectrophotometric protocol. However, this qualification approach is based on the absorption spectra and the object sample is the solid-state film, making it challenging to calculate the oxidized Spiro radical accurately and guide the precise design of the Spiro recipe. Incorporating the Spiro radical directly can control the doping molar ratio. However, this approach, which relies on the complex synthesis, is diffi-

cult to replace or be compatible with the conventional recipe of Spiro. 9,24 Therefore, it is highly desirable to propose a novel doping strategy with a precise and distinct mechanism to balance the high efficiency and high stability of PSCs by removing the residual Li<sup>+</sup> and precisely controlling the doping efficiency, which should also be significant for elucidating the influence of the doping state in the properties of Spiro and the corresponding device.

In this work, we proposed a novel doping strategy that is distinguished from the conventional doping mechanism to control doping efficiency accurately and avoid residual Li+ through electrolyzing, which is named electrolysis doping. Electrolysis doping utilizes the cleanest redox agents of electron and hole to oxidize the Spiro and reduce Li<sup>+</sup> respectively, leading to a Spiro radical and Li atom. This strategy can control the doping amount through regulating the electrolytic electricity. Different from the conventional doping process, the LiTFSI is served to assist the electrolysis as the ion compensation for charge conservation, in which the Li<sup>+</sup> can be removed through Li metal transformation, avoiding massive amounts of residual Li<sup>+</sup>. The resulting PSCs achieved efficiencies of >26% in regular PSCs using electrolyzed Spiro and >25.5% in inverted PSCs using electrolyzed poly[bis(4-phenyl) (2,4,6-trimethylphenyl)amine (PTAA). The regular device showed enhanced stability by maintaining ~97% of initial efficiency under  $\sim$ 25% relative humidity (RH) for 5,000 h. The inverted device can maintain 91% of its initial efficiency after operating under a onesun illumination in a N2 glovebox for 1,400 h. Besides, this electrolysis doping strategy, which does not rely on the chemical dopant, also supports decoupling the conductivity and Fermi-level tunability when combined with suitable chemical additives, providing a new way to modulate Spiro and other organic semiconductors in photoelectronic devices.

# **RESULTS AND DISCUSSION**

# Electrolysis doping strategy and its influence on Spiro electrical property

The organic charge transport material is one of the key materials to fabricate high-performance PSCs, among which, Spiro is a benchmark hole transport material in regular-structure devices, and PTAA is commonly used in both regular and inverted structural devices. 6,25,26 A drawback of these common organic semiconductors is the need for complex and time-consuming oxidation that relies on an ancillary oxidant and additive to realize optimal conductivity and Fermi level (Figure S1). As for Spiro, a large amount of LiTFSI is utilized to facilitate the generation of a Spiro radical with exposure to ambient air using oxygen as the oxidant, leaving massive residual Li<sup>+</sup> in final film. In addition, this oxidation process is usually complex, and the doping efficiency relies on the ambient condition and oxidation time, which makes it a challenge to quantify the doping efficiency and reveal the mechanism that is currently described in the equation shown in Figures 1A and S2. 12,27,28 Compared with conventional oxidation processes and the reported pre-oxidation strategy using chemical oxidants, 10-12 the hole as the oxidant is first utilized to pre-oxidize Spiro in an electrolysis strategy, which possesses a clear doping mechanism and well-controlled manner. It is noted that the electrolyzed organic semiconductor is called an





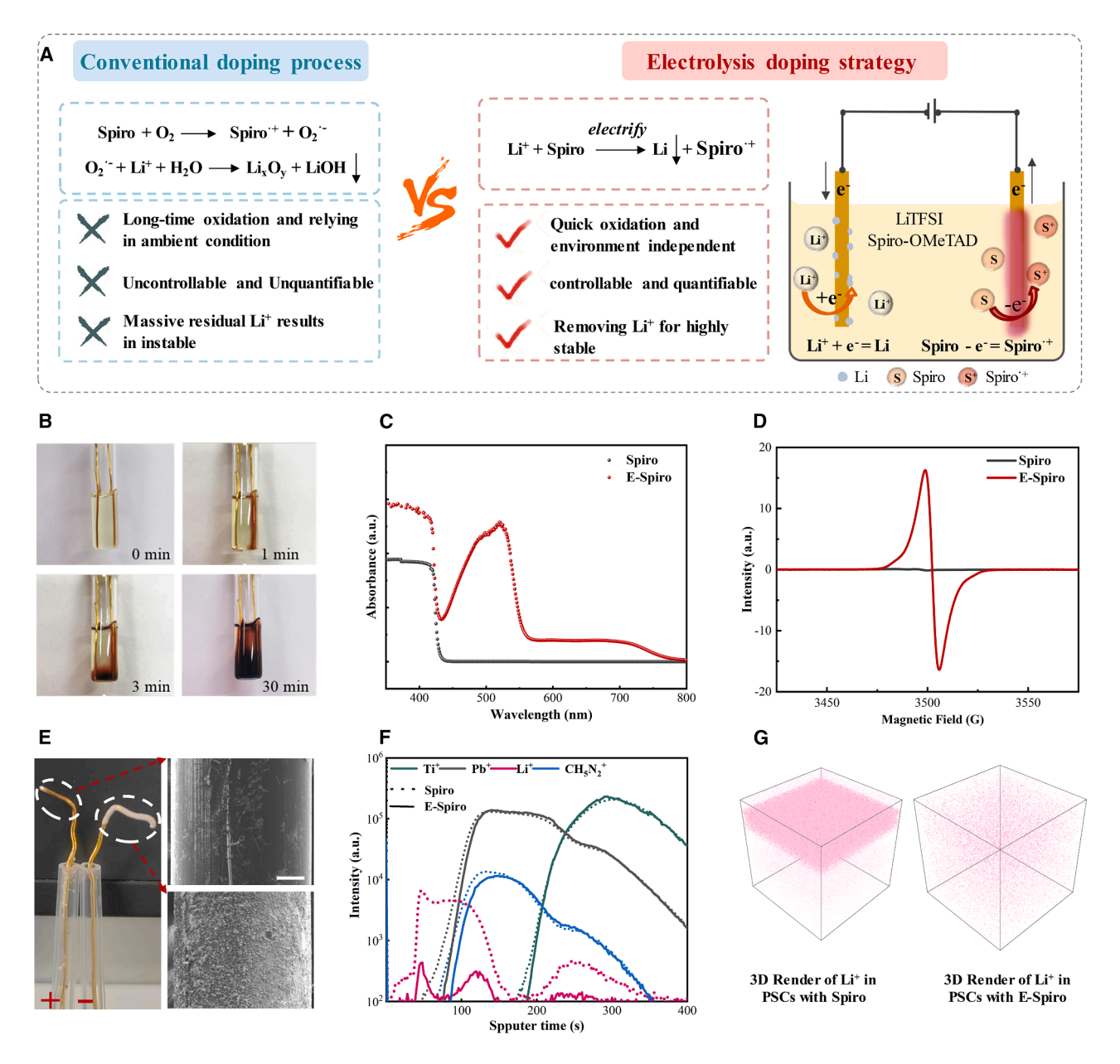


Figure 1. Electrolysis doping strategy and its influence on Spiro film

- (A) Schematic diagram of electrolysis doping strategy.
- (B) Photos of E-Spiro under different electrolysis times. The electrode was Au, and the applied bias voltage was 5 V.
- (C) The absorption spectra of Spiro and E-Spiro, the samples were solutions.
- (D) ESR spectroscopy of Spiro and E-Spiro, the samples were films.
- (E) The photos of anode and cathode electrodes and their corresponding SEM images. The scale bar was 100 µm.
- (F) The TOF-SIMs spectra of device with Spiro and E-Spiro. These devices were operated under one-sun illumination for 4 h before measurement.
- (G) 3D renders of Li<sup>+</sup> in devices with Spiro and E-Spiro.

E-semiconductor in this work, such as E-Spiro. In the electrolyte system, the dominated reactions on the surface of the anode and the surface of the cathode have been proposed to be the Spiro oxidation and the Li<sup>+</sup> reduction (Figure S3; Note S1). Notably, as for the electrolysis doping system, the LiTFSI plays an important role in assisting the electrolysis as an ion compensation for charge conservation and stabilizing the Spiro. In detail, as

shown in Figure 1A, on the anode electrode surface, the Spiro can be oxidized to a Spiro radical through losing electrons. Meanwhile, on the cathode electrode surface, the Li<sup>+</sup> can be reduced to a Li atom by accepting electrons, thus realizing the Spiro oxidation and removal of Li<sup>+</sup>. The pathways of charge transfer in the electrolyte system have also been analyzed (Figure S4). This elect'rolysis doping utilizes the hole as an





oxidant, enabling the doping process to deliver a controllable doping efficiency without incorporating any additional chemical additives, regardless of the ambient conditions.

We have determined the oxidation potential of Spiro be  $\sim$ 0.9 V, which was also consistent with previous reports 10,29 (Figure S3). To assure successful oxidation, we chose a bias voltage of 5 V to demonstrate the electrolysis doping strategy in a manner with a constant voltage charge using the LAND test system (Video S1), and we confirmed that this bias voltage shows a negligible influence on molecular structure of Spiro and other additives using measurements of Fourier transform infrared (FTIR) spectroscopy, X-ray photoelectron spectroscopy (XPS), and nuclear magnetic resonance (<sup>1</sup>H NMR) (Figures S5 and S6; Note S2). The Au electrode was also demonstrated to not dissolve during the electrolysis doping (Figure S7; Note S2). Figure 1B exhibits screenshots from a video, which is available in the supplemental information, of the electrolysis doping process with different electrolyzing times, indicating that the electrolysis treatment can effectively induce the oxidation of Spiro, and the oxidized Spiro is generated at the surface of the anode electrode. The experimental measurement of absorption spectra was used to characterize a Spiro solution, in which the spectrum of E-Spiro shows an absorption peak at roughly 520 nm, demonstrating the oxidized Spiro radical (Figure 1C). The absorption spectra of a Spiro film and E-Spiro film were also characterized (Figure S8). A peak located at roughly 520 nm emerged in the spectrum of the E-Spiro film. In addition, according to the absorption spectra, we calculated the band gap of the Spiro film and E-Spiro film to be 2.958 and 2.952 eV, respectively. The oxidized Spiro after electrolysis doping is also validated by the measurement of electron spin resonance (ESR), which can be supported by the emerged paramagnetic peaks at 3,480-3,520 G (Figure 1D). As for the chemical reaction on the surface of the cathode electrode, we speculate it should be that the Li+ is reduced to a Li atom, which can be demonstrated by the generation of Li metal that is observed directly (Figure 1E). Scanning electron microscopy (SEM) was utilized to observe the electrodes before and after electrolysis (Figures 1E, S9, and S10). Compared with the original Au surface and the anode electrode surface, the cathode surface is covered by Li<sub>x</sub>O<sub>x</sub>, generated from the exposure of metallic Li to air. The generated metallic Li and the subsequent oxidation can be demonstrated by XPS (Figure S11; Note S3). The generation of Li metal can remove the Li<sup>+</sup> from a Spiro solution, avoiding residual Li+ in the final film. Time-of-flight secondary ion mass spectrometry (TOF-SIMS) was carried out to confirm the non-residual Li<sup>+</sup> in E-Spiro (Figure 1F). As for the PSCs with Spiro, we can observe the Li<sup>+</sup> and its diffusion into and even across perovskite films.30 This long-range diffusion of Li+ has been reported to detrimentally damage device performance.<sup>30</sup> In comparison, we hardly capture the signal of Li<sup>+</sup> in the PSCs with E-Spiro, indicating the slight residual Li+. The corresponding three-dimensional (3D) renders of Li<sup>+</sup> in PSCs with Spiro and E-Spiro also confirm the removal of Li<sup>+</sup> from Spiro after electrolysis doping (Figure 1G). The Li removal can also be validated by the XPS results (Figure S12). The electrolysis doping strategy can effectively induce the oxidation of Spiro and reduction of Li<sup>+</sup> at the same time by leveraging the oxidation of hole and reduction of electron, respectively, which realizes the controllable oxidation of Spiro and removal of Li<sup>+</sup>.

To investigate the influence of electrolysis doping on the electrical properties of Spiro film, we first measured the conductivity of Spiro with different amounts of electricity during electrolysis based on the hole-only device structured as fluorine-doped tin oxide (FTO)/poly(3,4-ethylenedioxythiophene (PEDOT):polystyrene sulfonate (PSS)/Spiro or E-Spiro/Au. Drawing on Faraday's law of electrolysis, we can determine the molar amount of generated Spiro radicals directly by observing the electricity through the LAND test system. The linear relationship between the amount of reacted substance and the transferred electricity quantity has also been experimentally validated using inductively coupled plasma atomic emission spectrometry (ICP-AES) (Figure S13; Note S4). As shown in Figures 2A and 2B, the conductivity changes with the increment of the amount of electricity in electrolysis and can be divided into two stages. In the first stage, the film conductivity quickly increases from 4.26  $\times$  10<sup>-4</sup> to 8.12  $\times$  10<sup>-3</sup> mS/cm along with the amount of electricity increasing to 0.145 mAh for a 1 mL Spiro solution. In the second stage, the film conductivity shows a slight change along with the increment of the amount of electricity. In addition to the conductivity, the Fermi level, an important factor of HTL to determine the device performance, was also measured after electrolysis doping using ultraviolet photoelectron spectroscopy (UPS). According to the UPS spectra shown in Figures 2C and 2D, we calculated the Fermi level of Spiro and E-Spiro to be -3.27 and -3.43 eV respectively. Besides, we can also calculate the valence band maximum (VBM) of Spiro and E-Spiro to be -4.99 and -5.02 eV, respectively. The down shift of both Fermi level and VBM after electrolysis doping is beneficial for interfacial energy level matching, enhancing the splitting of quasi-Fermi level and promoting interfacial hole extraction (Figures S14 and S15).31 The measurement of Mott-Schottky analysis and time-resolved photoluminescence (TRPL) were utilized to explore the influence of electrolysis doping on interfacial carrier transport. As shown in Figure 2E, the PSCs with E-Spiro exhibit a built-in field ( $V_{\rm bi}$ ) of 0.93 V, which is higher than that of PSCs with Spiro (0.88 V), confirming the reduced energy level off-set. The higher  $V_{\rm bi}$  is beneficial for the separation of photo-generated electron-hole pairs and interfacial hole extraction. The TRPL spectra of samples structured as glass/ perovskite/Spiro (E-Spiro) was shown in Figure S16. Based on this TRPL spectra, we further computed the differential lifetime.<sup>32</sup> The charge transfer process at early times (until  $\sim$ 1  $\mu$ s) led to a sharp rise of  $\tau$ , the steepness of this rise was influenced by the charge transfer speed (Figure 2F). Analysis of the gradient for E-Spiro reveals a marked acceleration in hole transfer to the Au electrode relative to Spiro. This kinetic advantage is further evidenced by the early onset of saturation at 0.6 µs for E-Spiro, compared with the delayed 1.3 µs saturation observed in Spiro, demonstrating a significant divergence in their charge transport characteristics. Considering that the electrolysis doping strategy shows a negligible influence on the nanostructure of Spiro/perovskite interface (Figures S17 and S18), the increased  $V_{\rm bi}$  and promoted interfacial hole extraction should mainly result from the electrolysis doping. The optimized interfacial carrier dynamic can contribute to reducing voltage loss in PSCs, which is beneficial for improving the PSCs efficiency.





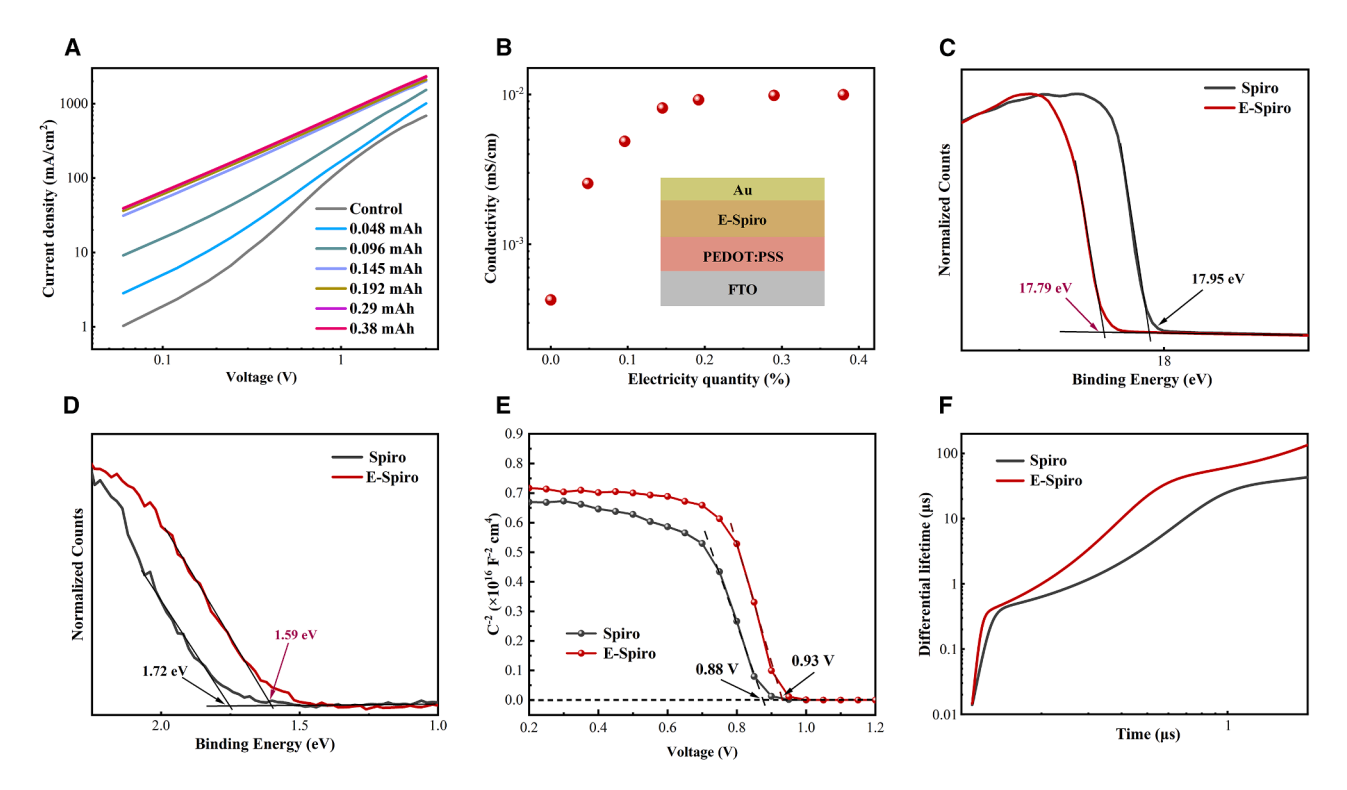


Figure 2. Effects of electrolysis doping on the electrical properties of Spiro
(A and B) *J-V* curves of hole-only devices and the corresponding calculated conductivity of E-Spiro with different amounts of electricity in electrolysis.
(C and D) UPS spectra of Spiro and E-Spiro films. The E-Spiro film was prepared after electrolyzing with 0.192 mAh for a 1 mL Spiro solution.
(E) Mott-Schottky curves of PSCs with Spiro and E-Spiro.

(F) Computed differential lifetimes through fitting the TRPL spectra.

The conventional Spiro needs a time-consuming oxidation process, normally in ambient air with controlled RH, to obtain an optimal conductivity and energy level structure, which makes the corresponding PSCs undergo a time period of storage to obtain optimal efficiency. In this oxidation process, the moisture in ambient air also participates in the reaction, 33 which brings a negative impact on the Spiro due to the moisture-sensitivity of lithium salts. Hence, precisely regulating the oxidation process of Spiro has been an effective approach to improve the efficiency and enhance the stability of PSCs. Based on this novel doping strategy, we monitored the power conversion efficiency (PCE) evolution of PSCs during the oxidation process of the HTL. As shown in Figure 3A, the PCE of PSCs with Spiro shows a typical increment as the oxidation time is prolonged, which is consistent with the previous reports. 10,34,35 This PCE evolution tendency is also shared by the PSCs with E-Spiro. Notably, the PCE of PSCs with E-Spiro shows a quicker increment as the oxidation time is prolonged and exhibits a higher reproducibility, which should result from the controllable and environment-independent electrolysis doping. In detail, the PSCs with E-Spiro can instantly obtain a PCE of more than 20%, and the PSCs with Spiro only obtain an instant PCE of less than 10%. The increased instant efficiency should result from the modified energy level structure and increased conductivity of E-Spiro, which can be evidenced by the theoretical calculation using the software Solar Cell Capacitance Simulator one- dimension (SCAPS-1D)

(Figures S19-S22; Note S5). It is observed that the PCE and open-circuit voltage (Voc) gaps between PSCs with Spiro and E-Spiro becomes smaller as the oxidation time increases and still exists after sufficient oxidation, which indicates that the electrolysis doping strategy can not only facilitate the rapid attainment of high efficiency but also contributes to the improvement in PSC efficiency (Figure S23). After sufficient oxidation, when using compact TiO<sub>2</sub> as the electron transport layer (ETL), the PSCs with E-Spiro obtain a champion PCE of 25.34% (short-circuit current density  $[J_{SC}] = 25.91 \text{ mA/cm}^2$ ,  $V_{OC} = 1.173$ V, and fill factor [FF] = 83.33%) with a satisfying reproducibility (Figures 3A and S24). In comparison, the PSCs with Spiro obtain a champion PCE of 24.91% ( $J_{SC} = 25.88 \text{ mA/cm}^2$ ,  $V_{OC} = 1.173 \text{ V}$ , and FF = 82.01%) (Figure 3B). The corresponding external quantum efficiency (EQE) was also measured, yielding an integrated  $J_{\rm SC}$  of 25.68 and 25.76 mA/cm<sup>2</sup> for PSCs with Spiro and E-Spiro, respectively, showing a small variation (<1%) from the values obtained from J-V measurement (Figure S25). The high efficiency obtained through the electrolysis doping strategy has also been validated by SnO2-based PSCs, which deliver a champion PCE of 26.16% with an average PCE of 25.67% (Figures 3C and S26). Impressively, the 26.16% achieved using E-Spiro with negligible residual Li+ was the highest value among the n-i-p PSCs with Li<sup>+</sup>-free HTL to date (Figure S27; Table S1).

Considering the distinct doping mechanism and the feature of being non-additive, the electrolysis doping strategy exhibits the



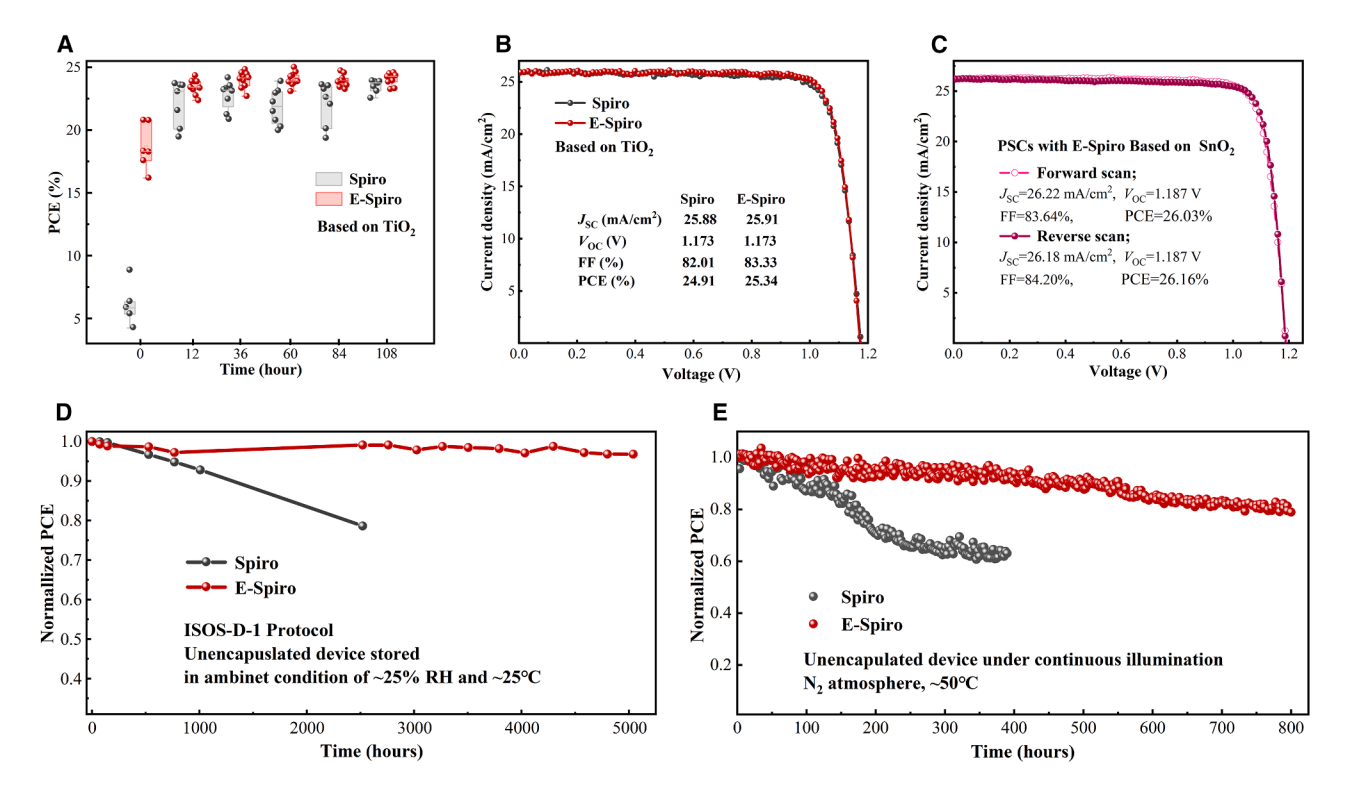


Figure 3. Photovoltaic performance of PSCs with Spiro and E-Spiro

- (A) PCE evolution of PSCs with different HTLs during the oxidation process in ambient air.
- (B) Reverse J-V curves of champion TiO<sub>2</sub>-based PSCs with Spiro and E-Spiro.
- (C) Reverse and forward J-V curves of champion  $SnO_2$ -based PSCs with Spiro and E-Spiro.
- (D) The long-term stability of unencapsulated devices stored in ambient conditions of  $\sim\!\!25\%$  RH and  $\sim\!\!25^{\circ}\text{C}.$
- (E) Operational stability of unencapsulated devices under continuous illumination in an  $N_2$  atmosphere.

potential to be compatible with the chemical-molecular regulation, further optimizing the device's photovoltaic performance and exploring the dedicated influence of additives on film property, especially the conductivity and Fermi level. We performed a comparative study of electrolytic doping and chemical doping using oxidants of I2 and dilaurylperoxide (DP), and the results show that the electrolysis doping strategy shows a similar ability with chemical doping in regulating the energy level structure of perovskite film, and a remarkable advantage in increasing the electrical conductivity (Figure S28). Based on this advantage in increasing conductivity and its non-additive feature, electrolysis doping is expected to be compatible with a chemical modulation strategy, which can regulate the Fermi level effectively, achieving an effective modulation on both conductivity and energy level structure (Figure S29). Based on the theoretical analysis and experimental exploration, we found that electrolysis doping can well be compatible with Co(III)-TFSI, an additive normally used in conjunction with LiTFSI in Spiro, which can further accelerate the achievement of optimal efficiency, leading to a PCE of over 25% that can be achieved immediately without going through air oxidation (Figures S30-S33; Note S6). Various measurements including conductivity tests, absorption spectra, and UPS indicate that the effectively modulated Fermi level of E-Spiro contributes to the improved instant efficiency, which is further support for obtaining high-efficiency PSCs with improved

reproducibility (Figures S34–S36; Note S7). These results demonstrate that electrolysis doping is able to accelerate and improve the achievement of PSCs' optimal PCE, which can be more than 26%, providing a new strategy to achieve high-efficiency PSCs. Furthermore, since the electrolysis doping delivers a distinct mechanism and has the feature of being non-additive, it exhibits a potential to decouple the conductivity and Fermi-level tunability when combined with suitable chemical additives, expanding the toolbox to develop novel HTL recipes and regulation strategies.

The Spiro HTL under conventional doping has been reported to show detrimental impacts on device stability, mainly due to the residual Li<sup>+</sup> that is hydrophilic and prone to migration. The electrolysis doping can achieve controllable pre-oxidation through an electrolyzed redox reaction with the participation of Li<sup>+</sup>, shortening the oxidation time in ambient air and removing the residual Li<sup>+</sup>, which is expected to enhance device stability. Before the device stability test, the stability of Spiro films was demonstrated to be enhanced through electrolysis doping (Figure S37). The contact angle of droplets on the perovskite/E-Spiro is higher than that of droplets on the perovskite/Spiro, which also shows the enhanced humid stability of Spiro (Figure S38; Note S8). Continuous monitoring of the efficiency evolution under long-term storage and operation was performed to assess the device stability. Figure 3D shows the long-term





stability of devices with Spiro and E-Spiro based on the ISOS-D-1 protocol.<sup>36</sup> The device with E-Spiro can maintain 97% of its initial efficiency with sufficient oxidation after storage in ambient air ( $\sim$ 25% RH and  $\sim$ 25°C) for 5,000 h, exhibiting enhanced storage stability. The enhanced storage stability under humid conditions can also be validated by SEM measurements of perovskite film after washing the Spiro HTL using chlorobenzene (CB). As shown in Figure S39, the obviously increased lead iodide (Pbl<sub>2</sub>) in perovskite film under Spiro has been observed after storage in a high-humidity condition of ~85% RH for 144 h, while the perovskite film under E-Spiro shows a slight increment of Pbl<sub>2</sub>. Furthermore, the operational stability of devices under continuous one-sun illumination in a N2 glovebox was also measured (Figure 3E). The device with E-Spiro can maintain ~81% of its initial efficiency after operating for 800 h, while the device with Spiro degraded to  $\sim$ 60% after operating for 400 h. Device stability under harsher conditions (higher humidity and higher temperature) has also been evaluated (Figure S40). Electrolysis doping can effectively enhance device stability under a condition of 25°C/45% RH. Although both types of device show an obvious efficiency decay in the conditions of  $85^{\circ}C$  and  $N_2$  atmosphere and  $85^{\circ}C$  and 85% RH, electrolysis doping can still show a positive effect on device stability. The removal of residual Li+ may mainly contribute to enhanced device stability, which inhibits Li<sup>+</sup> migration into the Au electrode under heat conditions and into the interior of perovskite films during the operation (Figures 1F, S41, and S42; Note S9).

# Universal application of electrolysis doping on organic semiconductors

The above results demonstrate that electrolysis doping can achieve controllable pre-oxidation of Spiro, which shows a mechanism distinct from conventional doping. This electrolysis doping leverages the oxidation of holes to oxidize the organic semiconductor. Since the oxidizing properties of holes can be well adjusted through controlling the bias voltage during the electrolysis process, the electrolysis doping is supposed to be applied across various semiconductors even though these materials possess different electrochemical characteristics. Before investigating the universal applicability of electrolysis doping to different materials, the feasibility of the electrolysis doping strategy on Spiro with different additives of Zn(TFSI)2, Cu(TFSI)2, Lithium bis (fluorosulfonyl)imideand (LiFSI), and 1-methyl-3-nonyl imidazolium bis(trifluoromethanesulfonyl)imide (OMIMTFSI) has been proved (Figure S43). In addition, the universal applicability of an electrolysis doping strategy to different perovskite components has also been validated, based on the PSCs based on MAPbl<sub>3</sub>  $MA_{0.75}FA_{0.25}PbI_3$  and  $MA_{0.84}FA_{0.1}Cs_{0.06}Pb(I_{0.89}CI_{0.11})_3$ , respectively (Figure S44).

We selected two common semiconductor materials, PTAA and poly(3-hexylthiophene-2,5-diyl) (P3HT), in PSCs to discuss the wild application of electrolysis doping. It is reported that both PTAA and P3HT can obtain a better electrical property through p-doping treatment. 16,37-39 As shown in Figures 4A and 4B, both the color changes of solution and the largely increased peak in electron paramagnetic resonance (EPR) spectra demonstrate that electrolysis doping can effectively oxidize P3HT and PTAA. The conductivity test was carried out

to validate the positive effect of electrolysis doping on the electrical properties of P3HT and PTAA (Figure S45). The doping mechanism of P3HT and PTAA was also analyzed (Figure S46). Moreover, the E-PTAA was further utilized as an HTL in regular n-i-p PSCs, achieving a champion PCE of 24.51% and average PCE of 24.22% (Figures 4C and S47), and in inverted p-i-n PSCs, it achieved a champion PCE of 25.57% and average PCE of 25.30% (Figures 4D and S48). When using an electrolysis strategy to fabricate inverted PSCs, we also evaluated the device stability. As shown in Figure 4E, the device based on E-PTAA can maintain 91% of its initial efficiency after operating for 1,400 h under continuous one-sun illumination in a N2 glovebox, showing excellent operational stability. The PTAA-based devices were also aged in harsh conditions of 25°C/45% RH, 85°C and N<sub>2</sub> atmosphere, and 85°C and 85% RH to evaluate device stability (Figure S49). Although the devices still show an obvious efficiency decay in conditions of 85°C and 85% RH, the device shows an enhanced humid stability and heat stability after electrolysis doping, maintaining almost 100% of their initial efficiency after 368-h aging in conditions of 25°C/45% RH and 85°C and N<sub>2</sub> atmosphere, respectively. The experimental results and discussion above demonstrate the feasibility of the electrolysis strategy in fabricating high-efficiency and stable PSCs with different structures and different hole transport materials.

#### **Conclusions**

In summary, an effective electrolysis doping strategy was proposed to modulate organic semiconductors in a controllable manner. The electrolysis doping leverages the redox agents of electrons and holes to selectively oxidize the Spiro to be Spiro radical and reduce Li<sup>+</sup> to Li metal, respectively, achieving a controllable oxidation and removal of Li+. Owing to the distinct mechanism that is based on electrolysis redox, the electrolysis doping strategy also shows a universal application in various organic semiconductors, such as Spiro, P3HT, and PTAA. We achieved a PCE of 26.16% using E-Spiro in a regular structure with significantly improved storage and operational stability, and a PCE of 25.57% using E-PTAA in an inverted structure with enhanced stability by maintaining 91% of initial efficiency after operating for 1,400 h under continuous onesun illumination. The electrolysis doping strategy shows a distinct mechanism with the remarkable advantage of Li+ removal, an increase in conductivity, and a non-additive feature, leading to a wild applicability and diversified strategies through combining the chemical doping strategy, which is expected to expand the applications of organic semiconductors on PSCs and other optoelectronic devices.

### **METHODS**

# Materials Substrates

The FTO glass (7  $\Omega$  sq<sup>-1</sup>) was purchased from Shangyang Solar Energy Technology.

Electron transport materials. Titanium tetrachloride (TiCl<sub>4</sub>) was purchased from Aladdin. Thioglycolic acid, urea, and tin (II) chloride dihydrate (SnCl<sub>2</sub>·2H<sub>2</sub>O) were purchased from Sigma-Aldrich.





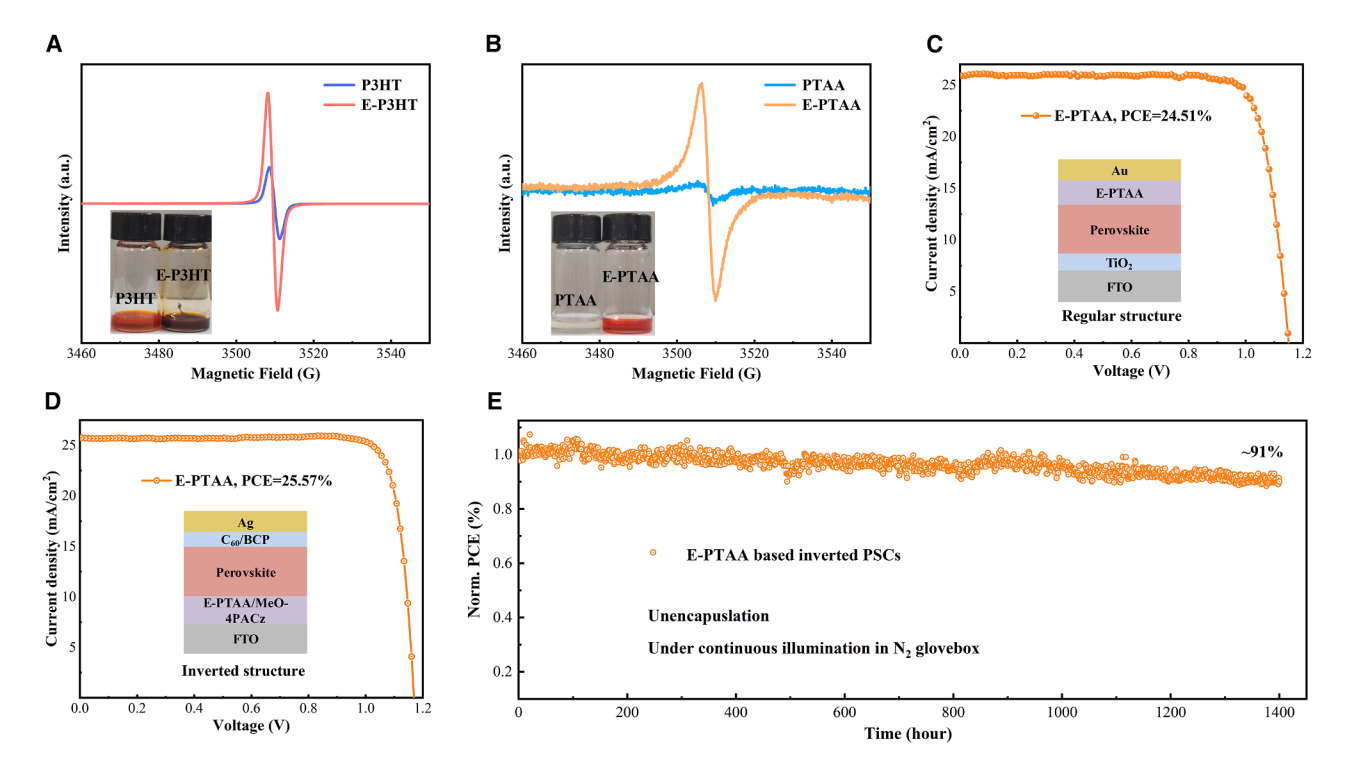


Figure 4. Universal application of electrolysis doping strategy

- (A) EPR spectra of P3HT and E-P3HT, the inset is the corresponding photos of P3HT and E-P3HT solutions.
- (B) EPR spectra of PTAA and E-PTAA, the inset is the corresponding photos of PTAA and E-PTAA solutions.
- (C) Reverse J-V curves of regular PSCs with E-PTAA, the inset is the schematic diagram of PSC structure.
- (D) Reverse J-V curves of inverted PSCs with E-PTAA, the inset is the schematic diagram of PSC structure.
- (E) Operational stability of unencapsulated inverted device with E-PTAA under continuous illumination in a  $N_2$  atmosphere.

Perovskite materials. Pbl<sub>2</sub> was purchased from Tokyo Chemical Industry (TCI). Rubidium chloride (RbCI) was purchased from Sigma-Aldrich. Formamidinium iodide (FAI), methylammonium chloride (MACI), and methoxy-Phenethylammonium iodide (MeO-PEAI) were purchased from Xi'an Yuri Solar. N, N-dimethylformamide (DMF), dimethyl sulfoxide (DMSO), and isopropanol (IPA) were purchased from Sigma-Aldrich.

Hole transport materials. Spiro, PTAA, LiTFSI, Co(III)-TFSI, and tert-butylpyridine (tBP) were purchased from Xi'an Yuri Solar. P3HT was purchased from Innochem. 4-Isopropyl-4 \( \'-\text{methyldiphenyliodonium} \) Tetrakis(pentafluorophenyl)borate was purchased from Aladdin. Acetonitrile (ACN) and CB were purchased from Sigma-Aldrich.

# **Device fabrication Substrate preparation**

The FTO substrate was sequentially ultrasonically cleaned with detergent, deionized water, ethanol, and deionized water for  $\sim\!15$  min, respectively. Then, the cleaned FTO substrate was dried by a  $N_2$  stream. The cleaned FTO was further processed under ultraviolet ozone (UVO) for 15 min to achieve a hydrophilic surface. Fabrication of a regular structured device

ETL preparation.  $TiO_2$  ETL preparation. 4 mL TiCl<sub>4</sub> and 200 mL deionized water were mixed to prepare the chemical bath precursor. Then, after the cleaned FTO substrate was immersed in precursor for 40 min at  $70^{\circ}$ C in a water bath.

 $SnO_2$  ETL preparation. 1.1 g  $SnCl_2 \cdot 2H_2O$  ( $\sim 12$  mM) and 5 g urea were dissolved in 400 mL deionized water, and then 5 mL HCl (37 wt %) and 100  $\mu$ L TGA were added into the urea solution to prepare the chemical bath precursor. Then, the cleaned FTO substrate was immersed into precursor for 4 h at 90°C in a drying oven. After the chemical bath, the sample was sequentially ultrasonically cleaned with deionized water and IPA for 5 min, respectively, followed by being annealed for 1 h at 150°C.

Perovskite film preparation. The perovskite film was fabricated by a two-step method. First, 1.5 M Pbl<sub>2</sub> (DMSO:DMF, 1:9 v/v) solution with 3% molar ratio RbCl was spin-coated on ETL at 1,500 rpm for 30 s, followed by annealing for 1 min at 70°C in a N<sub>2</sub> glovebox. Then, the ammonium salt (90 mg FAI and 13 mg MACI dissolved in 1 mL IPA) was spin-coated on PbI<sub>2</sub> film at 1,800 rpm for 30 s, followed by annealing for 15 min at 150°C in air condition (the RH should be controlled between 30%~40%). At last, the annealed perovskite film was transferred into a N<sub>2</sub> glovebox, and the MeO-PEAI solution (4.5 mg in 1 mL IPA) was spin-coated on perovskite film at 4,500 rpm for 30 s. HTL preparation. Spiro HTL preparation. For Spiro HTL, 72.3 mg Spiro with 26.6 µL tBP and 18 µL LiTFSI salt (520 mg/ mL in ACN) were mixed in 1 mL CB to prepare the Spiro solution, then this solution was spin-coated on top of a passivated perovskite film at 4,000 rpm for 30 s. For E-Spiro HTL, according to the designed doping molar ratio, the corresponding LiTFSI (normally 10% higher than the designed doping molar ratio) was added





into the Spiro solution and the added tBP also reduced according to the molar ratio of LiTFSI. Then, the Spiro solution was electrolyzed under a bias voltage of 5 V in a manner of constant voltage charge using the LAND test system, and the charged electricity was monitored to decide when to stop the electrolysis. After electrolysis, the E-Spiro was spin-coated on top of passivated perovskite film at 4,000 rpm for 30 s.

PTAA HTL preparation. The PTAA solution was prepared by mixing 30 mg PTAA, 1 mg 4-Isopropyl-4\footnote{-methyldiphenyliodonium Tetrakis(pentafluorophenyl)borate, and 1 mg dodecanoyl peroxide in 1 mL CB with 9  $\mu$ L tBP and 6  $\mu$ L LiTFSI salt (520 mg/mL in ACN), and then electrolyzed under a bias voltage of 3 V in a manner of constant voltage charge using the LAND test system, then was spin-coated on top of a passivated perovskite film at 4,000 rpm for 30 s, followed by annealing at 100°C for 5 min.

Au electrode preparation. Au electrode (60 nm) was deposited by thermal evaporation on top of HTL.

#### Fabrication of inverted-structured device

HTL preparation. The PTAA solution used in the regular structured device was diluted to 0.5 mg/mL, and then was spin-coated on cleaned FTO substrate at 4,000 rpm for 30 s, followed by annealing at 100°C for 5 min. Then, the MeO-PACz solution (0.4 mg/mL in IPA) was spin-coated on PTAA at 3,000 rpm for 30 s followed by annealing at 100°C for 10 min.

Perovskite film preparation. 1.5 M perovskite solution (FA $_{0.85-}$ MA $_{0.1}$ Cs $_{0.05}$ PbI $_3$  in a mixed solvent of DMF:DMSO with v/v of 4:1) was spin-coated on HTL at 1,000 rpm for 10 s and 5,000 rpm for 30 s. 200  $\mu$ L CB was dripped onto the center of the film at 5 s before the end of spin-coating. The deposited perovskite film was then annealed at 100°C for 30 min. Then, PEACI solution (1 mg/mL in IPA) was spin-coated on perovskite film at 4,000 rpm for 30 s, followed by annealing at 100°C for 3 min.

*ETL* preparation. C60 and BCP were deposited on top of passivated perovskite by thermal evaporation with thicknesses of 15 and 7 nm, respectively.

Ag electrode preparation. Ag electrode (100 nm) was deposited by thermal evaporation on top of ETL.

# Characterization

To characterize the oxidized Spiro, PTAA, and P3HT, ultravioletvisible (UV-Vis) spectra (SHIMADZU UV-2600) and EPR spectrometry (Bruker EMX PLUS) were carried out. To characterize the micro-surface of electrode and perovskite film, cold-fieldemission SEM (Hitachi S-4800) was performed. To characterize its existence and migration, TOF-SIMS (5-100, IONTOF GmbH) was performed. FTIR spectroscopy (Bruker) was performed on Spiro solution before and after electrolysis. The capacitancevoltage (C-V) measurement (AMETEK-Modulab XM) was performed to characterize the redox potential of Spiro. A platinum electrode was used as the counter electrode and the reference electrode was Ag/AgCl (saturated KCl). Ferrocene was added to the test solution as an internal standard to calibrate the potential. UPS (ESCALAB 250Xi) was carried out to characterize the Fermi-level structure of Spiro film. Mott-Schottky analysis was carried out on PSCs with different HTLs using an electrochemical workstation (Zahner Zennium). TRPL (Edinburgh Instrument, FLS980) was performed to characterize the interfacial carrier dynamic with an excitation wavelength of 470 nm. The TRPL fitted curves were obtained according to the following biexponential equation:

$$I(t) = A_1 \exp\left(\frac{-t}{\tau_1}\right) + A_2 \exp\left(\frac{-t}{\tau_2}\right)$$

where the fast decay time constants  $(\tau_1)$  correspond to radiative recombination processes and the slow decay time constants  $(\tau_2)$  correspond to nonradiative recombination processes.

Device efficiency was measured by using a Keithley 2400 source meter with a scanning rate of 65 mV/s under simulated AM 1.5 G illumination, and the mask area is 0.08 cm $^2$ . The EQE was measured by QE-R systems (Enli Tech). The operational stability tracking of the device was tested under light-emitting diode illumination (AM 1.5 G) in a N $_2$  glovebox.

#### **SCAPS-1D** introduction

SCAPS-1D v.3.3.11 was used in this work to build a PSC model, validating the effectiveness of the doping strategies employed. SCAPS-1D was developed by Marc Burgelman and his colleagues at the University of Gent, Belgium.

#### **RESOURCE AVAILABILITY**

#### Lead contact

Further information and requests for resources should be directed to and will be fulfilled by the lead contact, Meicheng Li (mcli@ncepu.edu.cn).

#### **Materials availability**

This study did not generate new unique materials.

# Data and code availability

This study did not generate any datasets.

#### **ACKNOWLEDGMENTS**

We thank Ligang Xu (Nanjing University of Posts and Telecommunications) for assistance in analyzing the <sup>1</sup>H NMR data. This work is supported partially by the National Natural Science Foundation of China (grant numbers 52402254, 52232008, 52102245, 52072121, and 22409061), Beijing Natural Science Foundation (grant numbers 2222076, 2222077, and Z240024), Beijing Nova Program (grant number 20220484016), Young Elite Scientists Sponsorship Program by CAST (grant number 2022QNRC001), the Fundamental Research Funds for the Central Universities (grant number 2024JC005), the project of China Three Gorges Corporation named key technologies of intelligent joint regulation and operation with grid connected friendly in power station group of wind, solar photovoltaic, and energy storage (grant number WWKY-2021-0173), Huaneng Group Headquarters Sci $ence \ and \ Technology \ Project \ (grant \ number \ HNKJ20-H88), the \ Fundamental$ Research Funds for the Central Universities (grant numbers 2024MS036, 2022MS029, 2022MS02, 2022MS031, 2023MS042, and 2023MS047), and the NCEPU "Double First-Class" Program.

## **AUTHOR CONTRIBUTIONS**

M.L. and H.H. conceived the idea. M.L. guided the work as a supervisor. H.H. and Z.L. did the experimental designs, device fabrication, and data analysis. Y.Y., H.Y., M.W., T.J., and B.L. participated in the device fabrication and some characterizations. C.S., S.Q., and Y.L. participated in film fabrication and some characterizations. H.H. wrote the first draft of the manuscript. Z.L., Y.Y., S.Q., Y.L., P.C., and M.L. assisted in revision and polishing the

Please cite this article in press as: Huang et al., Controllable electrolysis doping of organic semiconductors for stable perovskite solar cells, Joule (2025), https://doi.org/10.1016/j.joule.2025.102106





manuscript language. All authors discussed the results and contributed to the revisions of the manuscript.

#### **DECLARATION OF INTERESTS**

The authors declare no competing interests.

#### SUPPLEMENTAL INFORMATION

Supplemental information can be found online at https://doi.org/10.1016/j. joule.2025.102106.

Received: March 6, 2025 Revised: April 25, 2025 Accepted: August 7, 2025

#### **REFERENCES**

- He, R., Wang, W., Yi, Z., Lang, F., Chen, C., Luo, J., Zhu, J., Thiesbrummel, J., Shah, S., Wei, K., et al. (2023). Improving interface quality for 1-cm<sup>2</sup> allperovskite tandem solar cells. Nature 618, 80–86. https://doi.org/10.1038/ s41586-023-05992-y.
- Green, M.A., Ho-Baillie, A., and Snaith, H.J. (2014). The emergence of perovskite solar cells. Nat. Photonics 8, 506–514. https://doi.org/10. 1038/nphoton.2014.134.
- Cui, P., Wei, D., Ji, J., Huang, H., Jia, E., Dou, S., Wang, T., Wang, W., and Li, M. (2019). Planar p-n homojunction perovskite solar cells with efficiency exceeding 21.3%. Nat. Energy 4, 150–159. https://doi.org/10. 1038/s41560-018-0324-8.
- Yan, L., Huang, H., Cui, P., Du, S., Lan, Z., Yang, Y., Qu, S., Wang, X., Zhang, Q., Liu, B., et al. (2023). Fabrication of perovskite solar cells in ambient air by blocking perovskite hydration with guanabenz acetate salt. Nat. Energy 8, 1158–1167. https://doi.org/10.1038/s41560-023-01358-w
- Qu, Z., Zhao, Y., Ma, F., Mei, L., Chen, X.K., Zhou, H., Chu, X., Yang, Y., Jiang, Q., Zhang, X., and You, J. (2024). Enhanced charge carrier transport and defects mitigation of passivation layer for efficient perovskite solar cells. Nat. Commun. 15, 8620. https://doi.org/10.1038/s41467-024-52925-y.
- Liang, Z., Zhang, Y., Xu, H., Chen, W., Liu, B., Zhang, J., Zhang, H., Wang, Z., Kang, D.H., Zeng, J., et al. (2023). Homogenizing out-of-plane cation composition in perovskite solar cells. Nature 624, 557–563. https://doi. org/10.1038/s41586-023-06784-0.
- Huang, Z., Bai, Y., Huang, X., Li, J., Wu, Y., Chen, Y., Li, K., Niu, X., Li, N., Liu, G., et al. (2023). Anion-π interactions suppress phase impurities in FAPbl<sub>3</sub> solar cells. Nature 623, 531–537. https://doi.org/10.1038/ s41586-023-06637-w.
- Du, S., Huang, H., Lan, Z., Cui, P., Li, L., Wang, M., Qu, S., Yan, L., Sun, C., Yang, Y., et al. (2024). Inhibiting perovskite decomposition by a creeperinspired strategy enables efficient and stable perovskite solar cells. Nat. Commun. 15, 5223. https://doi.org/10.1038/s41467-024-49617-y.
- Zhang, T., Wang, F., Kim, H.B., Choi, I.W., Wang, C., Cho, E., Konefal, R., Puttisong, Y., Terado, K., Kobera, L., et al. (2022). Ion-modulated radical doping of spiro-OMeTAD for more efficient and stable perovskite solar cells. Science 377, 495–501. https://doi.org/10.1126/science.abo2757.
- Lan, Z., Huang, H., Du, S., Lu, Y., Sun, C., Yang, Y., Zhang, Q., Suo, Y., Qu, S., Wang, M., et al. (2024). Cascade reaction in organic hole transport layer enables efficient perovskite solar cells. Angew. Chem. Int. Ed. Engl. 63, e202402840. https://doi.org/10.1002/anie.202402840.
- Yang, H., Xu, T., Chen, W., Wu, Y., Guo, X., Shen, Y., Ding, C., Chen, X., Chen, H., Ding, J., et al. (2024). Iodonium Initiators: Paving the air-free oxidation of Spiro-OMeTAD for efficient and stable perovskite solar cells. Angew. Chem. Int. Ed. Engl. 63, e202316183. https://doi.org/10.1002/ anie.202316183.

- Ye, L., Wu, J., Catalán-Gómez, S., Yuan, L., Sun, R., Chen, R., Liu, Z., Ulloa, J.M., Hierro, A., Guo, P., et al. (2024). Superoxide radical derived metal-free spiro-OMeTAD for highly stable perovskite solar cells. Nat. Commun. 15, 7889. https://doi.org/10.1038/s41467-024-52199-4.
- Wang, S., Sina, M., Parikh, P., Uekert, T., Shahbazian, B., Devaraj, A., and Meng, Y.S. (2016). Role of 4-tert-butylpyridine as a hole transport layer morphological controller in perovskite solar cells. Nano Lett. 16, 5594– 5600. https://doi.org/10.1021/acs.nanolett.6b02158.
- Zhu, G., Yang, L., Zhang, C., Du, G., Fan, N., Luo, Z., Zhang, X., and Zhang, J. (2022). Unveiling the critical role of oxidants and additives in doped Spiro-OMeTAD toward stable and efficient perovskite solar cells. ACS Appl. Energy Mater. 5, 3595–3604. https://doi.org/10.1021/acsaem.1c04097.
- Cappel, U.B., Daeneke, T., and Bach, U. (2012). Oxygen-induced doping of spiro-meotad in solid-state dye-sensitized solar cells and its impact on device performance. Nano Lett. 12, 4925–4931. https://doi.org/10.1021/ pl302509g
- Kong, J., Shin, Y., Röhr, J.A., Wang, H., Meng, J., Wu, Y., Katzenberg, A., Kim, G., Kim, D.Y., Li, T.D., et al. (2021). CO<sub>2</sub> doping of organic interlayers for perovskite solar cells. Nature 594, 51–56. https://doi.org/10.1038/ s41586-021-03518-y.
- Saygili, Y., Kim, H.S., Yang, B., Suo, J., Muñoz-Garcia, A.B., Pavone, M., and Hagfeldt, A. (2020). Revealing the Mechanism of Doping of spiro -MeOTAD via Zn Complexation in the Absence of Oxygen and Light. ACS Energy Lett. 5, 1271–1277. https://doi.org/10.1021/acsenergylett. 0c00319.
- Xu, J., Shi, P., Zhao, K., Yao, L., Deger, C., Wang, S., Zhang, X., Zhang, S., Tian, Y., Wang, X., et al. (2024). Ion-migration inhibitor for spiro-OMeTAD/ perovskite contact toward stable perovskite solar cells. ACS Energy Lett. 9, 1073–1081. https://doi.org/10.1021/acsenergylett.4c00049.
- Tan, B., Raga, S.R., Chesman, A.S.R., Fürer, S.O., Zheng, F., McMeekin, D.P., Jiang, L., Mao, W., Lin, X., Wen, X., et al. (2019). LiTFSI-free spiro-OMeTAD-based perovskite solar cells with power conversion efficiencies exceeding 19%. Adv. Energy Mater. 9, 1901519. https://doi.org/10.1002/ aenm.201901519.
- Seo, J.Y., Kim, H.S., Akin, S., Stojanovic, M., Simon, E., Fleischer, M., Hagfeldt, A., Zakeeruddin, S.M., and Grätzel, M. (2018). Novel p-dopant toward highly efficient and stable perovskite solar cells. Energy Environ. Sci. 11, 2985–2992. https://doi.org/10.1039/C8EE01500G.
- Kim, S.G., Fish, G.C., Socie, E., Terpstra, A.T., Park, D.A., Zhu, K., Grätzel, M., Moser, J.E., and Park, N.G. (2024). Photo-doping of spiro-OMeTAD for highly stable and efficient perovskite solar cells. Joule 8, 1707–1722. https://doi.org/10.1016/j.joule.2024.03.012.
- Luo, J., Zhu, J., Lin, F., Xia, J., Yang, H., JinyuYang, J., Wang, R., Yuan, J., Wan, Z., Li, N., et al. (2022). Molecular doping of a hole-transporting material for efficient and stable perovskite solar cells. Chem. Mater. 34, 1499–1508. https://doi.org/10.1021/acs.chemmater.1c02920.
- Forward, R.L., Chen, K.Y., Weekes, D.M., Dvorak, D.J., Cao, Y., and Berlinguette, C.P. (2019). Protocol for quantifying the doping of organic hole-transport materials. ACS Energy Lett. 4, 2547–2551. https://doi. org/10.1021/acsenergylett.9b01766.
- Nguyen, W.H., Bailie, C.D., Unger, E.L., and McGehee, M.D. (2014). Enhancing the hole-conductivity of Spiro-OMeTAD without oxygen or lithium salts by using Spiro(TFSI)<sub>2</sub> in perovskite and dye-sensitized solar cells. J. Am. Chem. Soc. *136*, 10996–11001. https://doi.org/10.1021/ ia504539w.
- Ma, K., Sun, J., Atapattu, H.R., Larson, B.W., Yang, H., Sun, D., Chen, K., Wang, K., Lee, Y., Tang, Y., et al. (2023). Holistic energy landscape management in 2D/3D heterojunction via molecular engineering for efficient perovskite solar cells. Sci. Adv. 9, eadg0032. https://doi.org/10.1126/sciadv.adg0032.
- Sun, J., Ma, K., Lin, Z.Y., Tang, Y., Varadharajan, D., Chen, A.X., Atapattu, H.R., Lee, Y.H., Chen, K., Boudouris, B.W., et al. (2023). Tailoring molecular-scale contact at the perovskite/polymeric hole-transporting material

Please cite this article in press as: Huang et al., Controllable electrolysis doping of organic semiconductors for stable perovskite solar cells, Joule (2025), https://doi.org/10.1016/j.joule.2025.102106





- interface for efficient solar cells. Adv. Mater. 35, e2300647. https://doi.org/10.1002/adma.202300647.
- Liu, X., Zheng, B., Shi, L., Zhou, S., Xu, J., Liu, Z., Yun, J.S., Choi, E., Zhang, M., Lv, Y., et al. (2023). Perovskite solar cells based on Spiro-OMeTAD stabilized with an alkylthiol additive. Nat. Photonics 17, 96–105. https://doi.org/10.1038/s41566-022-01111-x.
- Abate, A., Leijtens, T., Pathak, S., Teuscher, J., Avolio, R., Errico, M.E., Kirkpatrik, J., Ball, J.M., Docampo, P., McPherson, I., and Snaith, H.J. (2013). Lithium salts as "redox active" p-type dopants for organic semiconductors and their impact in solid-state dye-sensitized solar cells. Phys. Chem. Chem. Phys. 15, 2572–2579. https://doi.org/10.1039/ c2cp44397j.
- Chen, Q., Wu, J., Wang, X., Li, G., Song, Z., Xu, Y., Deng, C., Weihai Sun, Y.D., and Lan, Z. (2022).
   3-Chloroperoxybenzoic acid doping spiroOMe-TAD for improving the performance of perovskite solar cells. Chem. Eng. J. 450, 138313. https://doi.org/10.1016/j.cej.2022.138313.
- Li, Z., Xiao, C., Yang, Y., Harvey, S.P., Kim, D.H., Christians, J.A., Yang, M., Schulz, P., Nanayakkara, S.U., Jiang, C.S., et al. (2017). Extrinsic ion migration in perovskite solar cells. Energy Environ. Sci. 10, 1234–1242. https://doi.org/10.1039/C7EE00358G.
- Caprioglio, P., Stolterfoht, M., Wolff, C.M., Unold, T., Rech, B., Albrecht, S., and Neher, D. (2019). On the relation between the open-circuit voltage and quasi-fermi level splitting in efficient perovskite solar cells. Adv. Energy Mater. 9, 1901631. https://doi.org/10.1002/aenm.201901631.
- Al-Ashouri, A., Köhnen, E., Li, B., Magomedov, A., Hempel, H., Caprioglio, P., Márquez, J.A., Morales Vilches, A.B.M., Kasparavicius, E., Smith, J.A., et al. (2020). 3-Chloroperoxybenzoic acid doping spiroOMeTAD for improving the performance of perovskite solar cells. Science 370, 1300– 1309. https://doi.org/10.1126/science.abd4016.

- Ding, C., Huang, R., Ahläng, C., Lin, J., Zhang, L., Zhang, D., Luo, Q., Li, F., Österbacka, R., and Ma, C.Q. (2021). Synergetic effects of electrochemical oxidation of Spiro-OMeTAD and Li<sup>+</sup> ion migration for improving the performance of n-i-p type perovskite solar cells. J. Mater. Chem. A 9, 7575–7585. https://doi.org/10.1039/D0TA12458C.
- Huang, H., Cui, P., Chen, Y., Yan, L., Yue, X., Qu, S., Wang, X., Du, S., Liu, B., Zhang, Q., et al. (2022). 24.8%-efficient planar perovskite solar cells via ligand-engineered TiO2 deposition. Joule 6, 2186–2202. https://doi. org/10.1016/j.joule.2022.07.004.
- Ma, F., Zhao, Y., Qu, Z., Yu, S., Chu, Z., Xiong, Z., Zhou, J., Wei, Z., Zhang, X., and You, J. (2023). Efficient perovskite solar cells with iodine-doped Spiro-OMeTAD hole transport layer via fast oxidation. Sol. RRL 7, 2300042. https://doi.org/10.1002/solr.202300042.
- Khenkin, M.V., Katz, E.A., Abate, A., Bardizza, G., Berry, J.J., Brabec, C., Brunetti, F., Bulović, V., Burlingame, Q., Di Carlo, A., et al. (2020). Consensus statement for stability assessment and reporting for perovskite photovoltaics based on ISOS procedures. Nat. Energy 5, 35–49. https:// doi.org/10.1038/s41560-019-0529-5.
- Liu, H., Zhang, Y., Huang, Z., Wu, Y., Wang, L., Liu, G., Chen, Y., Li, K., Zhang, W., and Zhou, H. (2024). Improved Charge-Transfer Doping in Crystalline Polymer for Efficient and Stable Perovskite Solar Cells. Adv. Energy Mater. 14, 2403737. https://doi.org/10.1002/aenm.202403737.
- Wang, T., Zhang, Y., Kong, W., Qiao, L., Peng, B., Shen, Z., Han, Q., Chen, H., Yuan, Z., Zheng, R., et al. (2022). Transporting holes stably under iodide invasion in efficient perovskite solar cells. Science 377, 1227– 1232. https://doi.org/10.1126/science.abq6235.
- Heo, J.H., Hong, S.Y., Park, J.K., Lee, H.J., Zhang, F., and Im, S.H. (2025). Chemical oxidization of PTAA enables stable slot-die-coated perovskite solar modules. Joule 9, 101850. https://doi.org/10.1016/j.joule.2025.101850.